Geophysical Journal International

Geophys. J. Int. (2025) **241,** 511–525 https://doi.org/10.1093/gji/ggaf057
Advance Access publication 2025 February 12
GJI Seismology

New insight into slow earthquake activities from continuous ocean bottom seismometers at the Guerrero seismic gap, Mexico

Yanhan Chen,[1] Yoshihiro Ito,[2] Raymundo Plata-Martinez,[3] Luis Antonio Dominguez,[3] Shukei Ohyanagi,[1] Emmanuel Soliman Garcia,[4] Ketzallina Flores,[1] Victor M. Cruz-Atienza,[3] Masanao Shinohara[5] and Yusuke Yamashita[2]

[1]*Division of Earth and Planetary Sciences, Kyoto University, kyoto,* 606-8502*, Japan. Email: chen.yanhan.m91@kyoto-u.jp*
[2]*Disaster Prevention Research Institute, Kyoto University, Uji, Kyoto,* 611-0011*, Japan*
[3]*Universidad Nacional Autónoma de México, Instituto de Geofísica, Ciudad de México,* 04510*, Mexico*
[4]*National Institute of Physics, University of the Philippines Diliman, Diliman, Quezon City,* 1101*, Philippines*
[5]*Earthquake Research Institute, The University of Tokyo, Tokyo,* 113-8654*, Japan*

Accepted 2025 February 10. Received 2025 January 23; in original form 2024 June 24

SUMMARY

The Guerrero seismic gap in the Mexican subduction zone exhibits a slip behaviour distinct from that of adjacent segments, which typically experience large earthquakes. With the acquisition of offshore seismic data in this region and the discovery of shallow tectonic tremors, the study of slow earthquakes has gradually increased. This study presents the detection of tectonic tremors and low frequency earthquakes (LFEs) in the Guerrero seismic gap using a combination of a modified envelope cross-correlation method and a matched filter applied to ocean bottom seismometer data for a continuous two-year observational period. The modified envelope cross-correlation method was used to detect and locate tremors, and the matched filter technique enabled the detection of LFEs. These methods allowed for better constraints on the depths of the detected events, offering new insights into tremors and LFE activity offshore the Guerrero seismic gap. Our results show that the spatial distribution of these phenomena, along with seismicity, residual gravity anomalies and seafloor topography, suggests that a section of the shallow plate interface within the gap has experienced stable slip. This study builds on previous work by enhancing the detection and location accuracy of these slow earthquakes, contributing to a more comprehensive understanding of subduction dynamics in the region.

Key words: Earthquake source observations; Episodic tremor and slip; Seismicity and tectonics; Subduction zone processes.

1 INTRODUCTION

Slow earthquakes, including slow slip events (SSEs), low-frequency earthquakes (LFEs) and tectonic tremors, are now well-recognized phenomena in subduction zones, significantly enhancing our understanding of fault slip behaviour (Obara & Kato 2016). These slow earthquakes provided crucial insights into the mechanics of subduction zones, such as Japan (Obara & Ito 2005; Asano *et al.* 2008; Ando *et al.* 2012; Matsuzawa *et al.* 2015; Arai *et al.* 2016; Nakamura 2017; Obara 2020; Takemura *et al.* 2023), Cascadia (Wech 2021; Gombert & Hawthorne 2023), Costa Rica (Brown *et al.* 2009; Baba *et al.* 2021) and Mexico (Kostoglodov *et al.* 2010; Husker *et al.* 2012; Frank *et al.* 2013; Cruz-Atienza *et al.* 2015; Villafuerte & Cruz-Atienza 2017; Cruz-Atienza *et al.* 2018). Particularly, they revealed the mechanisms of fault slip behaviour and stress accumulation-release processes along the plate interface. In some cases, shallow slow earthquakes have been reported to trigger both moderate and large earthquakes, as observed in the Japan Trench before the Tohoku-Oki earthquake (Kato *et al.* 2012; Ito *et al.* 2013, 2015; Uchida *et al.* 2016).

LFEs are typically characterized by their short-duration, impulsive nature with low frequency content, while tremors are prolonged signals with low amplitude and emergent characteristics. Tectonic tremors have proven to be an invaluable tool for identifying and monitoring SSEs and their evolution (Rogers & Dragert 2003; Hirose & Obara 2005; Bartlow *et al.* 2011; Villafuerte & Cruz-Atienza 2017; Itoh *et al.* 2022). LFEs and tectonic tremors are key components of subduction zones, offering valuable information on fault mechanics and earthquake dynamics. In many regions, LFEs are used to pinpoint the locations of tremors, and their occurrence is often linked to episodic slip along the plate interface. However, the relationship between LFEs and tremors can be complex, as they do not always overlap in space or time. This complexity is particularly pronounced in regions, such as Mexico, where the connection between these phenomena remains an area of active investigation.

In the Mexican subduction zone, SSEs have been extensively documented, but their relationship with LFEs and tremors is still not fully understood. While tremors typically accompany SSEs and share similar locations (Beroza & Ide 2011), not all slow slips coincide spatially and temporally with tremors in Cascadia (Wech & Bartlow 2014). This complexity is especially evident in the Mexican subduction zone (Husker *et al.* 2012; Frank *et al.* 2014; Villafuerte & Cruz-Atienza 2017; Cruz-Atienza *et al.* 2018; Husker *et al.* 2019; Plata-Martinez *et al.* 2021). Previous studies from Shikoku and the San Andreas Fault have demonstrated a close association between LFEs and tremors, with LFEs being more easily identifiable due to their distinct *P*- and *S*-wave onsets (Shelly *et al.* 2007; Frank *et al.* 2013). However, such a connection has not been observed clearly in the offshore portion of the Guerrero gap, where tremors have been detected without corresponding shallow LFEs. Shallow, near-trench LFEs are not as common as deep LFEs. Takemura *et al.* (2023) pointed out the difficulty of shallow LFEs detection. It is not easy to distinguish LFEs and tremors due to thick low-velocity sediments at the shallow plate boundary. Understanding this discrepancy about the shallow LFEs occurrence is critical, as the relationship between LFEs and tremors may offer new insights into strain accumulation and release in slow slip areas.

The subduction zone in Mexico has been responsible for significant earthquakes over the past century, notably the impactful Mw 8.0 Michoacán earthquake in 1985, which resulted in the tragic loss of over 10 000 lives in Mexico City (Beck & Hall 1986; UNAM Seismology Group 1986; Kanamori *et al.* 1993). However, there is a notable exception known as the Guerrero seismic gap. This specific segment of the Mexican subduction zone has not experienced M7 + earthquakes since 1911 (Singh *et al.* 1981; Yoshioka *et al.* 2004; UNAM Seismology Group 2015). Instead, it has been characterized by large and relatively shallow slow-slip events (Kostoglodov *et al.* 2003; Radiguet *et al.* 2012; Radiguet *et al.* 2016; Cruz-Atienza *et al.* 2021). Thus far, the unique pattern of strain accommodation and, therefore, the slip behaviour observed in the Guerrero gap, which differs from adjacent segments where significant earthquakes occur regularly, is not fully understood.

Tremors and LFEs in the Guerrero gap have been widely studied in relation to long- and short-term SSEs occurring in deep onshore segments of the plate interface (Payero *et al.* 2008; Kostoglodov *et al.* 2010; Frank *et al.* 2013; Cruz-Atienza *et al.* 2015; Villafuerte & Cruz-Atienza 2017; Cruz-Atienza & Villafuerte *et al.* 2018). Offshore tremor observations, however, were only made possible following the deployment of ocean bottom seismometer (OBS) in 2017 (Cruz-Atienza & Ito *et al.* 2018). Plata-Martinez *et al.* (2021) made a breakthrough by identifying shallow tectonic tremors offshore in the Guerrero seismic gap using OBS data, marking the first detection of tremors in this region. To date, no shallow LFEs have been detected in Mexico, likely due to observational limitations and the challenging nature of these events. Given that LFEs are considered a component of tremor, understanding their dynamics is essential for gaining deeper insights into the behaviour of tremors and slow slip in the plate interface (Shelly *et al*. 2006).

Plata-Martinez *et al.* (2021) used the models of global bathymetry and gravity anomaly models (Bassett & Watts 2015a, b) to explain the tremors phenomena in the Guerrero seismic gap. Residual gravity anomalies can provide insights into the structure and density variations within the Earth's crust, which in turn may relate to the occurrence of slow earthquakes, such as those found in the seismic gap. The large positive and negative residual gravity anomalies are also interpreted as an irregular subducting relief that increases pore pressure and fracturing and decreases coupling, generating shallow tremors (Plata-Martinez *et al.* 2021). Building on the work of Plata-Martinez *et al.* (2021), this study delves deeper into the relationship between LFEs and tremor by using both OBS data and onshore seismic networks for a continuous period of two years, which is twice as long as the period analysed by Plata-Martinez *et al.* (2021). Our objective is to clarify how these phenomena interact, particularly in offshore regions where observations have been sparse. By refining detection methods for LFEs and tremors, we aim to shed light on the processes governing slow earthquakes in the Guerrero gap and contribute to a broader understanding of slow slip behaviour in subduction zones.

2 DATA AND METHODS

2.1 Data

We used continuous data from ocean bottom seismometers (OBS) at a two-year-long array of stations deployed in 2017 November throughout the offshore portion of the Guerrero seismic gap (Cruz-Atienza & Ito *et al.* 2018). The array was located between the Guerrero shoreline and the Middle American Trench, and data were analysed from 2017 November to 2019 November. An additional OBS was deployed in the second year to complete the seismic array with eight units (OBS10, Fig. 1).

The OBS stations were equipped with three-component 1 Hz short-period sensors and deployed at water depths ranging between 980 and 2350 m. Station locations were determined with an average uncertainty of 2 m and the data were corrected using time-shifts and instrumental responses.

We collected information about earthquakes in this area. For earthquakes with magnitudes of 5 or higher since 1976, we adopted focal mechanisms provided by the Global Centroid Moment Tensor (GCMT) agency. However, due to the systematic bias of event locations by this agency in the region of about 15–20 km to the northeast (Hjörleifsdóttir *et al.* 2016; Singh *et al.* 2019), we adopted more reliable hypocentres determined by the National Seismological Service, the Geophysics Institute of the National Autonomous University of Mexico (SSN, 2018) from its local broad-band seismic network.

2.2 Modified envelope correlation method

The initial identification of tremors within the subduction zone of western Japan was accomplished using the envelope correlation method (Obara 2002). This method examines the similarity of envelope waveforms recorded at various seismic stations. It locates the source of tremors by elucidating the observed differences in traveltimes for tremor signals, achieved by optimizing the cross-correlations of envelope waveforms. These traveltimes were calculated based on ray theory. The precise location of a tectonic tremor poses challenges because of the absence of characteristic impulsive body wave arrivals on which conventional earthquake-location techniques rely. Although more sophisticated location methods have been proposed (Hendriyana & Tsuji 2021; Akuhara *et al.* 2023), we adopted an improved version of the technique introduced by Mizuno & Ide (2019), to detect and locate tremors; it is based on a maximum likelihood method that is sufficiently fast, accurate, and applicable to large databases.

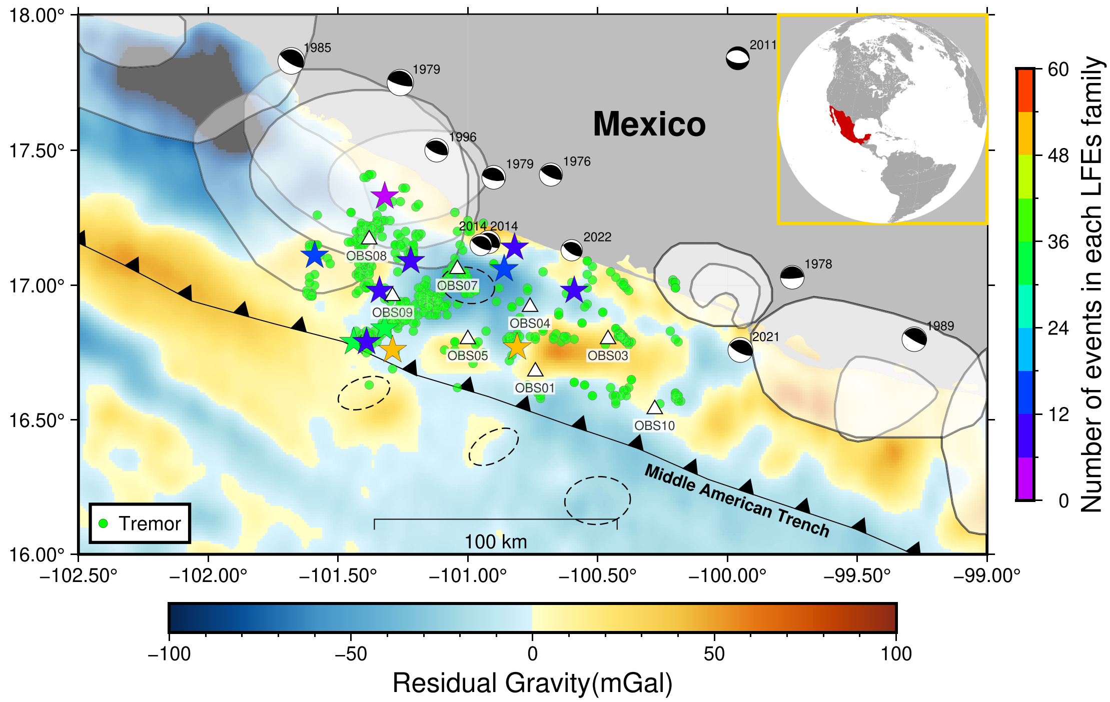

Figure 1. Map view of the study area in the Guerrero seismic gap. Triangles show the location of eight ocean bottom seismometers (OBSs). Circles represent tectonic tremors. Stars whose colour changes with the rightmost colour bar series represent the LFEs family, and different colours indicate the number of LFEs in each family. Residual Gravity anomalies are from Plata-Martínez *et al.* (2021). The four dashed circles in the figure represent seamounts from left to right: Koyuki, Popped-up, Ender and Yoshi seamounts (Černý *et al.* 2020). The transparent circles represent the rupture areas of earthquakes that have occurred over the past few decades.

To estimate the envelope waveforms, we carried out the following steps: (1) band-pass filtering of continuous velocity data between 2 and 8 Hz, (2) squaring of the filtered data, (3) low-pass filtering at 0.3 Hz, and (4) resampling of the filtered signal at 1 Hz. The square root of those filtered data was adopted as envelope. For tremor detection, 300-second time windows with 150-second time steps were used. The detection threshold for the cross-correlation coefficient between stations was set to 0.6 (Ide 2010).

For the analysis, we examined a collection of continuous envelope waveforms derived from seismograms with a sampling interval ΔT. The objective was to identify tremors within a fixed time window with a width $T_\mathrm{w} = N_\mathrm{t}\Delta T$, where N_t represents the number of time samples. Within this time window, we define the normalized envelope waveform as $w_i(t)$. Thus, the timing of the tremor windows for all components at each station is

$$w_i(t) = \frac{w_i'(t)}{\sqrt{\sum_{k=1}^{N_\mathrm{t}} \left(w_i'(t_k) - \overline{w_i'}\right)^2}} \quad (1)$$

where the sub-index i represents the i-th component, $w_i'(t)$ is the original envelope waveform, $\overline{w_i'}$ is the temporal mean, N_t is the number of time samples, and t_k is the k-th time step in the window. In our method, we assumed that the shape of the envelopes was consistent across all components and stations. As a result, each tremor observation, denoted as the normalized envelope waveform $w_i(t)$, can be modelled as the sum of a common template waveform $w(t)$ after applying a common moveout, Δt_i, associated with the traveltimes from the source, and a Gaussian error term $e_i(t)$ following a distribution $N(0, \sigma_i^2)$. Mathematically, this relationship can be expressed as:

$$w_i(t + \Delta t_i(x)) = w(t) + e_i(t + \Delta t_i(x)) \quad (2)$$

where $\Delta t_i(x)$ is the traveltime from a potential source position x to the station recording the i-th component.

Under these assumptions, we can formulate mathematical expressions to maximize the likelihood when detecting the observed envelopes by combining a common template waveform $w(t)$ and the traveltimes to a specific position x. The maximum likelihood problem can be solved by calculating the weighted sum of the cross-correlations, where the weights are determined by the error variance. Consequently, we aim to maximize the average of the weighted cross-correlations, also known as the average weighted cross-correlation (ACC),

$$ACC(x) = \frac{\sum_{(i,j)} \sum_{k=1}^{N_t} \frac{w_i(t_k + \Delta t_i(x)) w_j\left(t_k + \Delta t_j(x)\right)}{\sigma_i^2 \sigma_j^2}}{\sum_{i,j} \frac{1}{\sigma_i^2 \sigma_j^2}} \quad (3)$$

The error variance was determined by assessing the similarity between the template and the observed waveforms. In this method, the objective is to identify the optimal tremor location x^{best} that maximizes ACC. To achieve this, traveltimes to various positions x were computed using ray theory and a modified 1D velocity model specific to the Guerrero region (Obana *et al.* 2003; Spica *et al.* 2016; Espindola-Carmona *et al.* 2021). Around offshore areas, due to the influence of sedimentary layers, the Vp Vs^{-1} ratio typically exceeds 1.73 (Bell *et al.* 2016; Chow *et al.* 2022). The Mexican subduction zone is characterized by a thick sedimentary layer on the landward slope of the trench. We integrated data on the sedimentary layer thickness and referred to the Vp Vs^{-1} values in the Nankai Trough (Obana *et al.* 2003) and crustal models in the Mexican region (Spica *et al.* 2016; Espindola-Carmona *et al.* 2021) to construct 1-D velocity models. The subsurface structure is shown in Supporting Information (Fig. S1).

To identify the optimal tremor locations, we employed a combination of grid search and gradient methods. Assuming a fixed tremor depth of 10 km, the grid search explored multiple positions and selected several local maxima of the ACC as potential tremor epicentre locations. It is important to note that we focused on the local maximum rather than the global maximum because multiple tremors may occur at different locations within the same time window. Thus, local maxima may indicate the presence of multiple tremors within a single time window.

After identifying candidate locations from the grid search, we used the conservative convex separable approximation (CCSA) algorithm (Svanberg 2002) to refine the locations. This method was similar to gradient descent in that it iteratively improves the hypocentre coordinates (epicentre and depth) by optimizing the ACC. CCSA is specifically chosen because it handles the convex optimization problem effectively and was capable of handling separable objective functions, making it ideal for this type of waveform-fitting problem. Each potential tremor epicentre served as an initial value for the algorithm, enabling the determination of the best hypocentre location for each tremor. In cases where hypocentre solutions from different potential locations were very close to each other, we combined these solutions to obtain a unified result.

We eliminated outliers by establishing two conditions that detected tremors must satisfy. First, the cross-correlation coefficients must be greater than the initial threshold of 0.6, as originally proposed. Secondly, the similarity between the envelope and template waveforms should be significant. If the correlation coefficient was below 0.4, the corresponding envelopes were rejected as outliers.

Once outliers were excluded, the location procedure was iterated using the gradient method and continued until no further outliers were identified. In addition to the gradient-based refinement, bootstrapping (Efron 1979) is used to assess the uncertainty of the determined hypocentre locations. In bootstrapping, we resampled the waveform data multiple times and repeated the location process for each resampled data set. This helps us to estimate the variability of the hypocentre solutions due to data noise or other factors. The standard deviation of the hypocentre parameters (latitude, longitude, depth) is then computed from the distribution of solutions across the bootstrap iterations. The standard deviations of the tremor location were approximately 1.5 km horizontally and 4.5 km vertically.

Fig. 2 shows an example of a tremor detected at the seven OBS stations. The first three stations clearly record the tremor signal, while signals at other stations become stretched due to propagation path effects. For detection and location, as long as three stations clearly record the signal, the event can be localized. Once the location of the tremor was identified, the waveforms at different stations were plotted with increasing epicentral distances.

The hypocentre time, duration and energy for each detected tremor were determined as follows:

$$\dot{E}_{\mathrm{s}}(t) = 4\pi\rho\beta \frac{\sum_{i,j}\left(\frac{w_i'^{2}\left(t+\Delta t_i\left(x^{\mathrm{best}}\right)R_i^2\right)}{\sigma_i^2} + \frac{w_j'^{2}\left(t+\Delta t_j\left(x^{\mathrm{best}}\right)R_j^2\right)}{\sigma_j^2}\right)}{\sum_{(i,j)}\left(\frac{1}{\sigma_i^2}+\frac{1}{\sigma_j^2}\right)}, \quad (4)$$

where $\dot{E}_{\mathrm{s}}(t)$ is the average seismic energy rate, R_i is the hypocentre distance to the station recording the i-th component, ρ and β are the density and *S*-wave velocity at the station, which are assumed as $\rho = 3000$ kg m$^{3\ -1}$and $\beta = 2.844$ km s $^{-1}$.

The hypocentre time was defined as the time at which maximum $\dot{E}_{\mathrm{s}}(t)$ occurred. The tremor duration was also estimated as the time at which $\dot{E}_{\mathrm{s}}(t)$ exceeded a quarter of its maximum value. Because of the local site effect at the stations, the amplitudes of the recorded waveforms may lack a common reference. The invalid rigidity assumption also causes additional overestimation of seismic energies for shallow tremors (Takemura *et al.* 2024a). Therefore, the magnitudes of the events were not considered in the analysis.

The described detection method demonstrated efficient performance even in cases, where multiple events occurred within the same time window. In windows with overlapping events, the method detected all occurrences, validating its ability to function with offshore data. However, as noted in Plata-Martínez *et al.* (2021), it remains challenging to distinguish between different types of seismic signals, such as tremors, earthquakes and T-phases (Okal 2008; Plata-Martínez *et al.* 2021; Takemura *et al.* 2024b). This limitation stems from the similarity in waveforms and the potential overlap in the frequency content of these events. For example, both tremors and T-phases can produce continuous, low-frequency signals, making it difficult to rely on automated detection alone for precise event classification.

To isolate tremors from earthquakes and other signals, we incorporated a visual inspection. This involved analysing both spectrograms and waveforms for each detection, ensuring a more accurate classification. Fig. 3 illustrates the typical appearance of an event during this inspection, highlighting key characteristics that differentiate tremors from other seismic events. The filtered signal of tectonic tremor presents a long duration spindle shape, fluent in tens to hundreds of seconds, shorter can be in a few seconds. There is no obvious *P* or *S* arrivals even in the 2–8 Hz filtered signal. In the spectrogram, the energy is low above 10 Hz. Together these characteristics are the basis we used to validate the tremor detections. By visually examining the frequency content and signal duration, we were able to identify patterns that automated methods might miss, improving the reliability of the detection results.

2.3 Matched filter technique

There are several different methods to detect LFEs: the matched filter method (Gibbons & Ringdal 2006; Shelly *et al.* 2007; Peng & Zhao 2009), polarization analysis (Maceira *et al.* 2010) and the statistical method (Ide 2021). The matched filter approach is a technique employed to find LFEs (Tang *et al.* 2010; Frank *et al.* 2013; Chamberlain *et al.* 2014). The waveform similarities are the basics of the matched filter technique. In this approach, the observed waveforms of known LFEs were employed as templates to cross-correlate with continuous waveform data to search for similarities. Detection is achieved when the accumulated cross-correlation function exceeds a pre-defined threshold.

We visually inspected the waveform and spectrogram within the detected tremor to find possible LFE templates as the initial templates and then cross-correlated them through continuous data (Shelly *et al*. 2006; Shelly *et al*. 2009; Frank *et al.* 2013).LFEs were identified as isolated events in tremor sequences. The horizontal components are easier to identify due to the LFEs' principally shearing motions (Shelly *et al*. 2006; Husker *et al.* 2012; Frank *et al.* 2013). Fig. 4 is one example of an initial inspection for a possible LFE template. Fig. S4 (Supporting Information) is an example showing LFE within tremor in the horizontal components and the vertical component. The signal is more notable in the horizontal components than in the vertical one. The LFE obtained from tremor with initial location is shown in Fig. S5 (Supporting Information).

Following the initial detection run, new LFE templates with relatively high signal-to-noise ratios were generated by stacking the

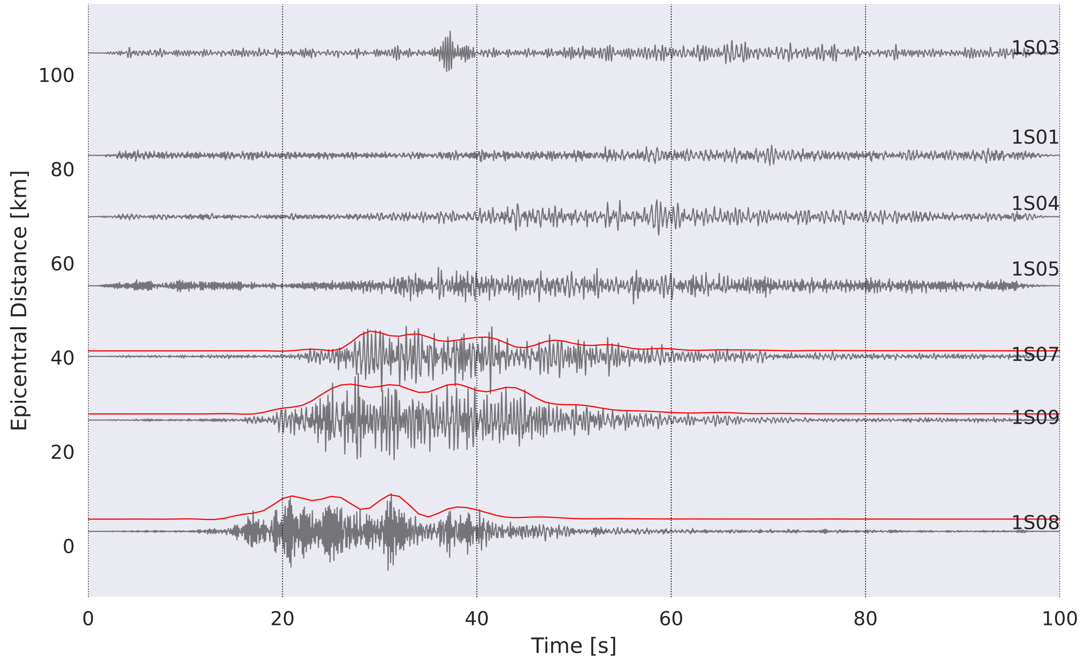

Figure 2. Example of one tectonic tremor seismogram as a function of the epicentral distance. In this example, due to the weak tremor signals, the waveforms of only three stations were significant. The smoothed line is a tremor's envelope.

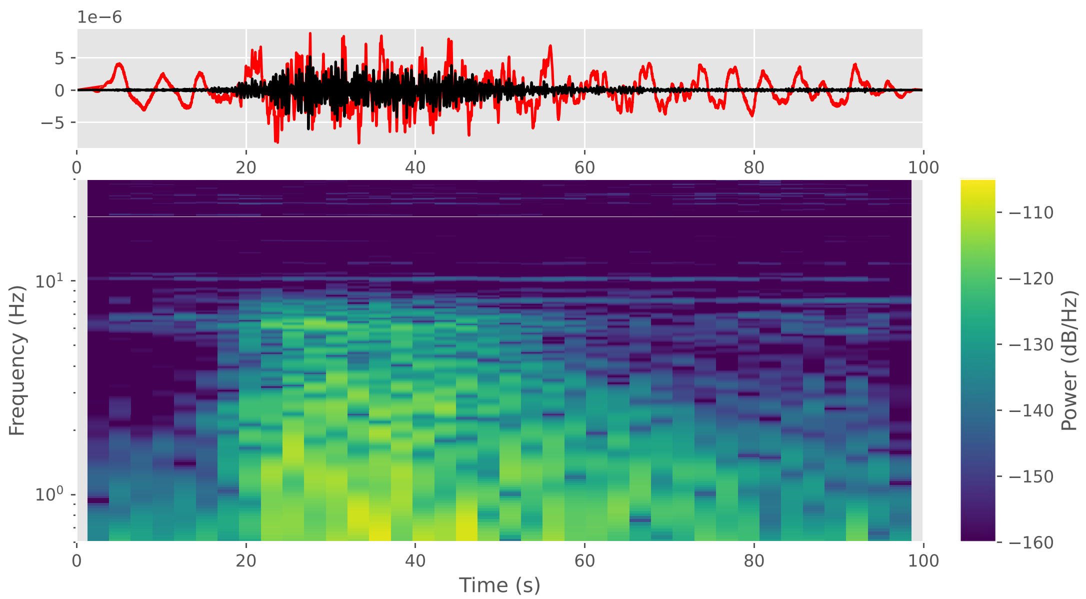

Figure 3. Waveform and spectrogram of a tremor. In the waveform plot, the cluttered trace represents the original waveform, while the spindle-shaped trace corresponds to the waveform after applying a 2–8 Hz bandpass filter. The spectrogram below illustrates the frequency content of the original waveform.

waveforms at the same station and component (Fig. 5). Stacking was linear, with each template normalized in amplitude (Thurber *et al.* 2014). As shown in Fig. 5, the waveforms before stacking can hardly be seen as obvious *P* or *S* phases. After stacking is performed, however, the *P* and *S* phases clearly emerge in the horizontal components while the *P* phase is even clearer in the vertical component. Moreover, as expected, the amplitude of the horizontal components is higher than that of the vertical component, which is consistent with the fact that LFEs are mainly generated due to shear rupture (Ide *et al*. 2007; Supino *et al.* 2020). What we also need to be aware of is that the site amplification coefficients in the horizontal components are typically larger than those in vertical components (Yabe *et al.* 2019, 2021; Takemura *et al.* 2024a), and so the site amplification differences between horizontal and vertical components in OBS recordings require attention.

The hypocentre of the detected LFE was assigned the same value as the corresponding template. These LFEs are considered to repeat at the source (Chamberlain *et al.* 2017). For some templates

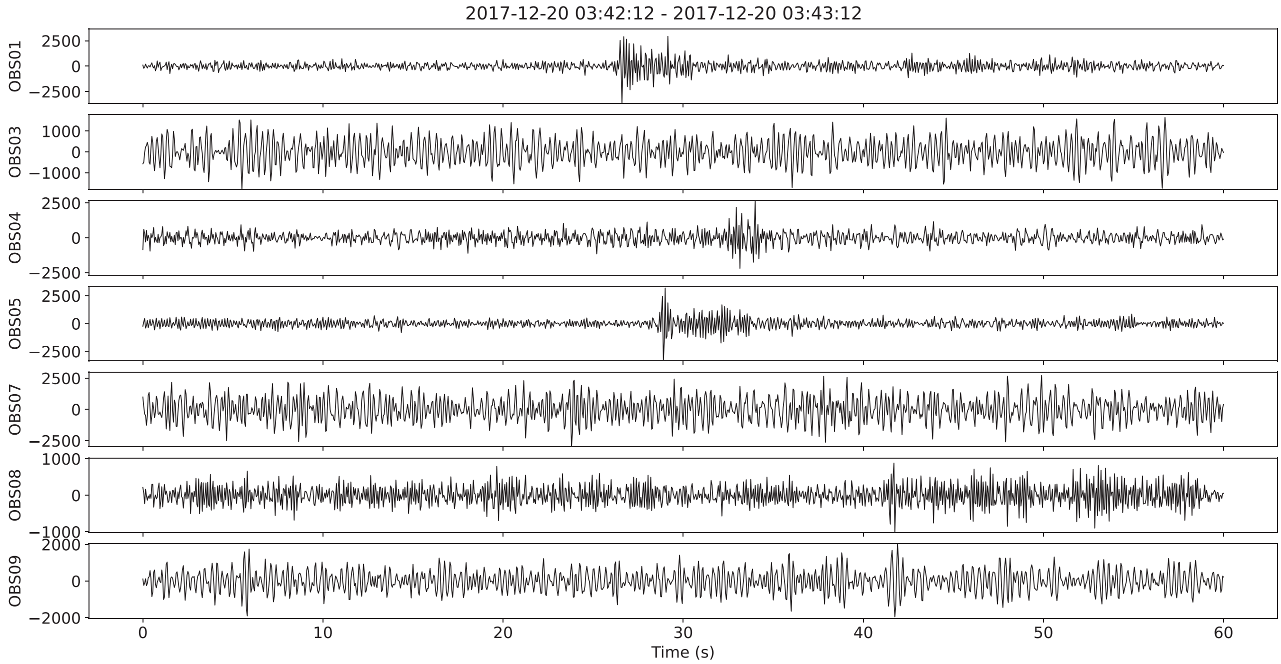

Figure 4. Visual inspection for a possible LFE template waveform at different stations during the initial detection stage. The start time is from 2017 December 20 03:42:12. The arrivals of the possible LFE are around 30 s. These show records for one of the horizontal components.

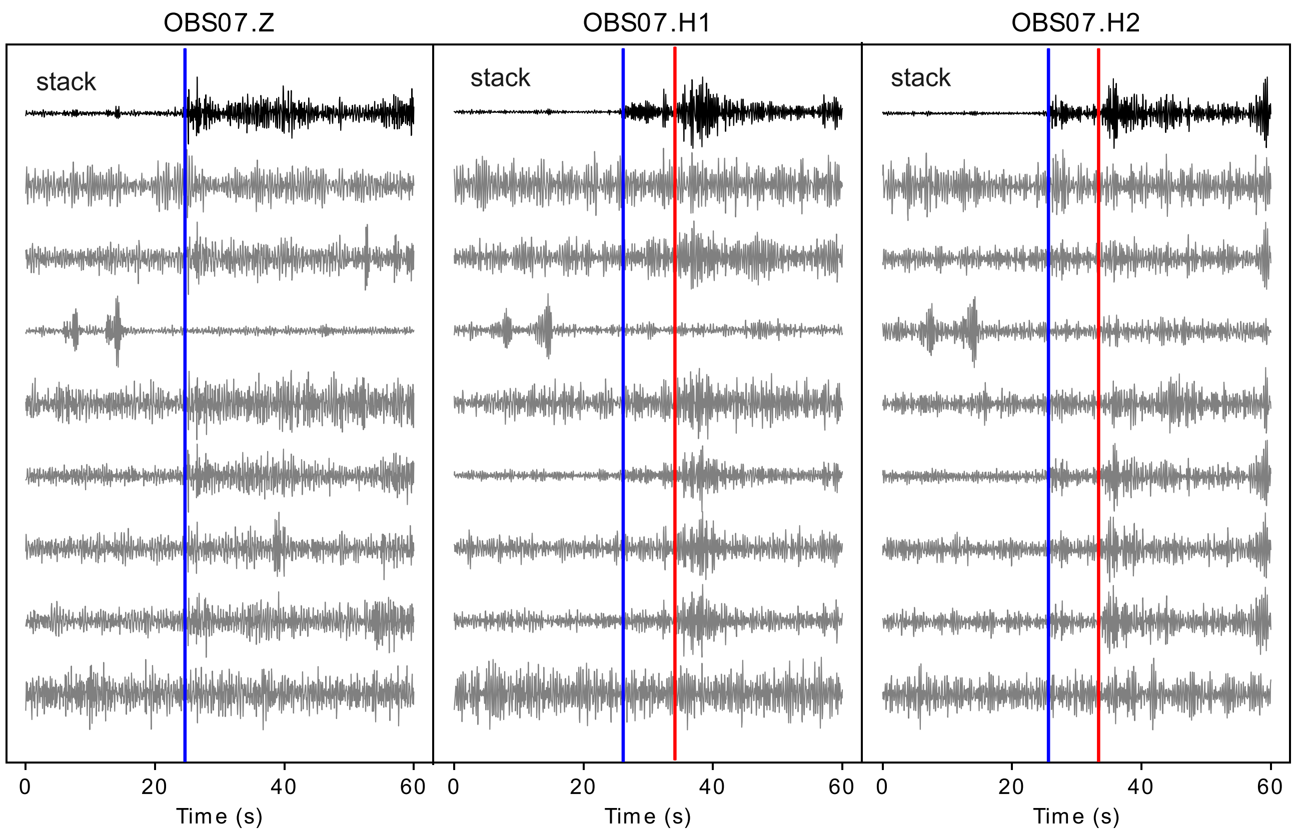

Figure 5. Example of a three-component LFE waveform with stacking. The first waveform of each subgraph represents the stacked LFE waveform, and the each waveform at the beginning of the second and thereafter is the individual LFE used to perform the stacking on the same station and the same component. OBS07 is the station code. *Z* is vertical component, and *H*1, *H*2 are horizontal components, respectively. The vertical line in the plot of the *Z* component is the arrival of the *P* wave, the vertical lines at the same positions in the *H*1 and *H*2 components are also the arrival of the *P* wave, and the other vertical lines in the *H*1 and *H*2 components are the arrival of the *S* wave.

with lower signal-to-noise ratios, this process of stacking and cross-correlation is iterated two to three times until the set of detected events and associated waveform stacks are stabilized (Shelly 2017). After confirming the stacked waveform templates, all the waveforms were cross-correlated using continuous data.

To accelerate the subsequent computations, we initially down-sampled all raw continuous waveforms from 200 to 20 Hz. We then applied a fourth-order, two-way bandpass filter with a frequency range of 2–8 Hz to both the continuous and template seismograms. Subsequently, we calculated the correlation coefficient (CC) value within a time window of 6 s between the template and continuous data.

To filter out noisy traces and reduce false detections, we assessed the signal-to-noise ratio (SNR) for all traces by examining a signal window of 1 s before and 5 s after the arrival time of either the *P* or *S* waves. A noise window of equivalent duration ending 1 s prior to the *P*-wave arrival was also analysed. We only included template events that presented at least 12 traces with SNRs exceeding 3. The analysis proceeded with a step size of one data point (0.05 s), aligning the CC values with the original time of the template event and calculating the average CC value across all channels at each data point. To reduce the uncorrelated background noise and amplify the signals of the LFEs, these shifted functions were stacked. To identify new detections, we set a threshold of 12 times the median absolute deviation of the daily mean CC functions (Meng *et al.* 2013; Yao *et al.* 2017; Beaucé *et al.* 2018). The detection is considered a new LFE if the stacked CC function surpasses this threshold. A summary of the workflow is provided in the Supporting Information (Fig. S3).

After detecting the LFEs using the matched filter technique, we estimated their hypocentre locations. To achieve this, we employed the WIN system (Urabe 1992) for manual phase picking and hypocentre calculation of the LFE families. The WIN system is a comprehensive processing platform for analysing multichannel seismic waveform data, featuring a suite of UNIX-compatible programmes, including the hypocentre determination tool hypoMH (Hirata & Matsu'ura M 1987). *P*- and *S*-wave arrival times were manually selected and the hypocentres were calculated using hypoMH, assuming a modified local 1-D velocity model (Fig. S1, Supporting Information) considering a sedimentary surface layer (Obana *et al.* 2003; Spica *et al.* 2016; Espindola-Carmona *et al.* 2021).

3 RESULTS

We compared the spectra of stacked waveforms of regular earthquakes, tectonic tremors, LFEs, and ambient noise recorded at the same station (Fig. 6). The distinct spectral characteristics of each event type are evident. The spectra for earthquakes demonstrate either increasing or stable energy levels up to around 10 Hz. In contrast, LFEs and tremors exhibit a steady decline, or at least constant energy from the lower frequencies onward. LFEs display significantly higher energy than noise. LFE and tremor spectra are highly similar, but tremors have larger amplitude. This reduction in energy at higher frequencies is a defining feature of LFEs and tremor. Although the variations present in the geological environment across different regions can influence the spectral characteristics of these signals, it is generally possible to distinguish between them. This capability of differentiating signals is consistent with the characteristics of LFE, tremors and regular earthquakes previously identified in other regions (Shelly *et al.* 2007; Beroza & Ide 2011).

A total of 637 tremors with durations ranging from 5 to 300 s were identified. The spatial distribution of these events is illustrated in Fig. 7 (colour coded circles) and the Supporting Information (Fig. S6). These results include short-duration tremors (Poiata *et al.* 2018; Toh *et al.* 2023). The uncertainties of tremor location were confined to within 1.5 km horizontally and 4.5 km vertically. Tremor predominantly occurred at depths of 8–23 km, as depicted in the depth histogram in Supporting Information (Fig. S2).

However, the depth estimates for these tremors are subject to significant limitations. First, the locations were calculated based on *S*-wave traveltimes, without incorporating *P*-wave traveltimes. Second, the velocity model employed for tremor location did not account for the low-velocity sedimentary layers present on the ocean floor. This omission is critical because the sedimentary layer significantly influences the traveltimes of seismic waves from the source to the OBS positioned above this layer. The absence of these considerations likely introduces additional inaccuracies in our locations, particularly affecting the depth. As a result, there was a systematic bias, leading to hypocentres deeper than the actual depths. Consequently, depth remained the least reliable parameter for tremor locations.

We employed a set of 12 LFE templates to detect events throughout the continuous data for the first year 2017–2018. Consequently, 205 LFEs were detected and located with an uncertainty of approximately 3 km. These LFEs were predominantly distributed in the northwestern part of the OBS array (colour coded stars), exhibiting a higher density near OBS8 and OBS9 (Fig. 7). Notably, several LFEs located south of OBS9 were proximal to the trench, suggesting that they may have been triggered by slow-slip transients in this very shallow zone. The regional distribution of LFEs was consistent with the observed tremor activity at depths ranging from 5 to 15 km. We show all the LFEs families in the Table 1.

Analysis of the cross-section showed that the depths of LFEs increased with distance from the trench compared with tremors. This pattern suggests the influence of inherent errors in tremor calculations. Despite these errors, we expect consistency between the observed depths of tremors and LFEs (e.g. Shelly *et al.* 2007). These discrepancies are primarily attributable to limitations of the cross-correlation method used for tremor localization. This method, which relies on the maximum amplitude of the tremor envelope, offers less precision than traveltime measurements of direct *P* or *S* waves utilized for LFEs. In contrast, the location of the LFEs involves the calculation of both the *P*- and *S*-wave arrival times, providing more accurate focus information. LFEs depth is therefore more reliable than that of tremors.

4 DISCUSSION

In general, tectonic tremors could be explained by the superposition of successive LFEs (Ide *et al*. 2007; Brown *et al.* 2009), while shallow LFEs observed in this study were not always accompanied by tremors. Soon after station deployment, in 2017 November, we detected a cluster of LFEs in the southwestern part of the OBS array, very close to the trench (Fig. 8a). One month later, LFE activity in the same spots sharply decreased and remained stable, similar to other clusters for the rest of the period (Fig. 8b). In Fig. 8(a), significant LFE activity can be observed in 2018 February. This is consistent with the tremor activity of Husker *et al.* (2019) in temporal distribution. The Husker *et al.* (2019) tremor catalogue uncovers additional seismic transients, including post-seismic slip in Oaxaca following the 2018 February 16 Mw 7.2 Pinotepa Nacional earthquake.

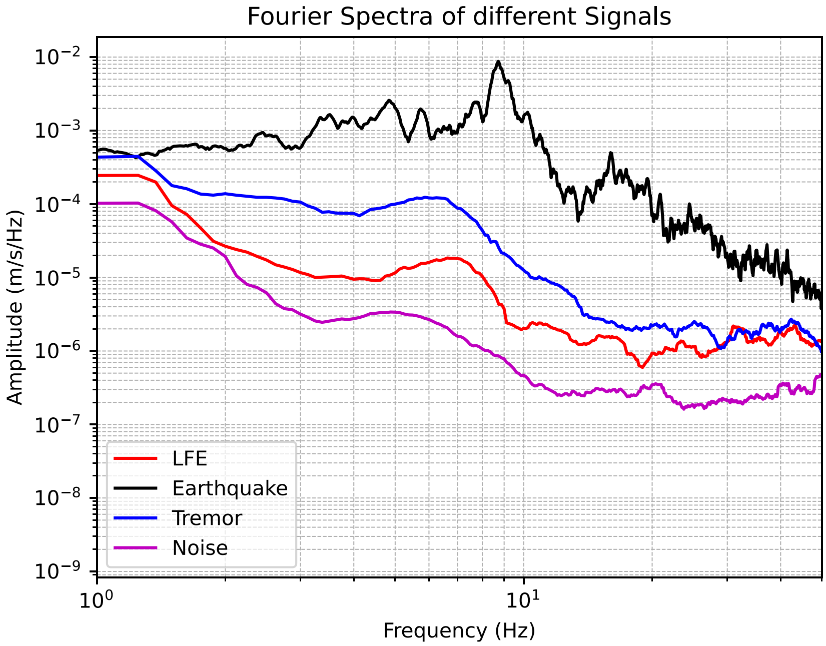

Figure 6. Comparison of the earthquake, LFE and tremor spectra. A comparison of stacked raw waveforms from the OBS seismogram's horizontal components is shown. The three signals are selected from approximately the same hypocentre region. We selected a 3-s time window to calculate their spectra.

At many plate boundaries, the transition zone between seismogenic and stable slip conditions results in slow earthquakes, including slow-slip events. Tremors usually occur together with SSEs and their locations are similar (Beroza & Ide 2011), whereas not all slow slips coincide spatially and temporally with tremors (Wech & Bartlow 2014). Previous knowledge of tectonic tremors and LFEs indicates that the two occur coherently; however, there are some special cases where LFEs occur without tremor activity. A similar phenomenon was observed in the Cascadia subduction zone, where Wech and Barlow (2014) concluded that there is a slip rate threshold for tremor genesis in the plate boundaries. Although our detected LFEs occur primarily along the slab interface, some LFEs were not associated with tremor catalogues. This pattern, similar to observations in Guerrero where Frank *et al.* (2014) found only 18.3 per cent of LFEs occur during tremor episodes, and only 35.4 per cent of tremors contain LFEs, suggests complex source mechanisms.

Shallow slow earthquakes in Costa Rica occurred near the trench axis, but they are separated from repeating and tsunami earthquakes (Baba *et al.* 2021). Arai *et al.* (2016) discussed the structure of the tsunamigenic plate boundary and shallow LFEs at the southern Ryukyu Trench. The LFE distribution at the Ryukyu trench seems to bridge the gap between the shallow tsunamigenic zone and the deep slow slip region. In the Guerrero gap, slow tsunamigenic earthquakes previously occurred near the trench (Iglesias *et al.* 2003). These earthquakes exhibit low-frequency characteristics and generate tsunamis. While some LFEs in this study are primarily found deeper along the subduction interface, given that these LFEs occur in a region (Iglesias *et al.* 2003) identified as prone to tsunami earthquakes, besides one possible reason above that the slip rate threshold effect for tremor, Since not all LFEs are found within tremors, we consider that the LFEs not detected in tremors may be related to small tsunami earthquakes, especially those occurred near the trench. LFEs associated with tremors are more likely to be linked with slow slip events, while LFEs not associated with tremors near the trench, are likely linked to slow tsunamigenic LFEs. These LFEs might share the slow rupture and low-frequency signature of tsunamigenic earthquakes, even if they are not currently recognized as such.

The LFEs families detected in this study indicated the existence of a shallow transition zone from creep to locking in the Guerrero seismic gap. Worldwide, most slow earthquakes occur updip and downdip from the locked seismogenic zone of the subducting plate interface in the so-called slip transition zones (Dixon *et al.* 2014; Todd *et al.* 2018; Nishikawa *et al.* 2019; Baba *et al.* 2020; Obara 2020; Takemura *et al.* 2020a). This supports the most widely accepted idea that LFEs are minor thrust ruptures that release tectonic stress next to or at the subduction interface (Ide *et al.* 2007; Shelly *et al.* 2007; Ohta & Ide 2011; Frank *et al.* 2013). At this interface, the two plates interact, creating complex geological conditions that lead to LFE activity (Ohta & Ide 2011). The LFEs families identified in this study were located in the shallow portion of the subducting interface near the trench. Some LFEs were observed near the coastline (Fig. 7). Between the LFEs near the trench and those close to the coastline, there is a low residual gravity anomaly, which was associated with a 'silent zone' where the interface may creep, as proposed by Plata-Martínez *et al.* (2021). From our observations, which include LFEs and tremors for a two-year period, although slow earthquakes are more frequent to the west, as found by these authors (i.e. west of longitude −101°), it is also clear that they disseminate across the study region with prominent clustering, some of which likely delineate subducted seamount trajectories, as discussed below. Places with no activity were relatively scarce. The −101° meridian roughly bounds the end of the seismic gap, west of which at least four Mw ≥ 7.2 ruptures have occurred in the past. (i.e. in 1943, 1979, 1985 and 2014) (UNAM Seismology Group 2015). Therefore, the sharp increase in slow earthquakes around this boundary may indicate an along-strike transition zone of the plate interface that prevents most large earthquakes from penetrating the gap. This suggests that LFEs and tremors concentrate around

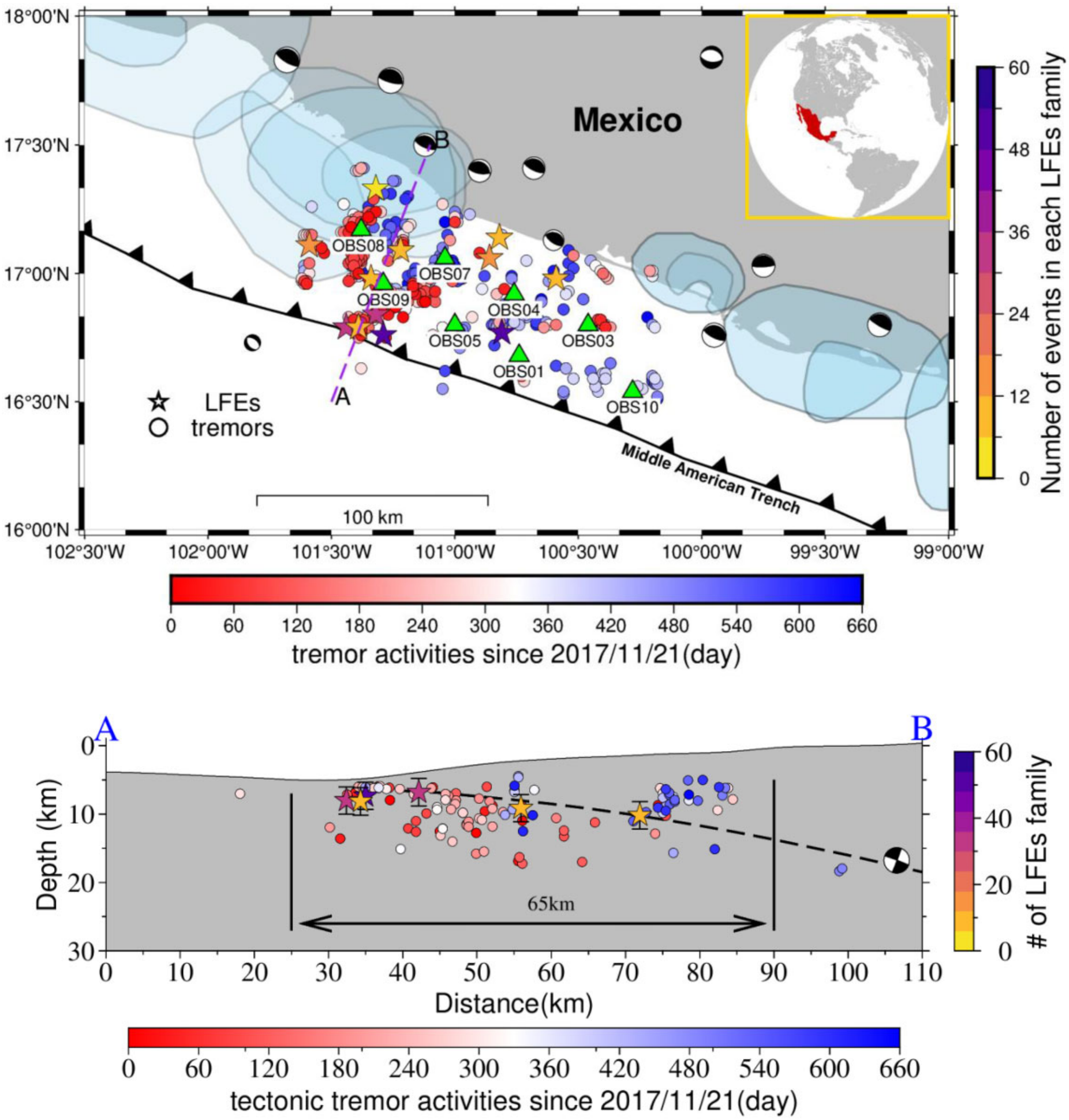

Figure 7. Migration of tremors activities for two years and cross-section in profile AB according to the width of 20 km. The different coloured circles represent the time when the tremor occurs. The slab is based on Slab 2.0 (Hayes *et al.* 2018). The source of the focal mechanism solutions shown in the figure is from GCMT. The transparent circles represent the rupture areas of earthquakes that have occurred over the past few decades.

Table 1. All the LFE families. The first three columns are latitude, longitude and depth, and the fourth column is the number of events detected per LFEs family.

Lat	Lon	Depth	Count
16.77	−100.81	8.21	60
17.33	−101.32	10.14	6
16.79	−101.44	9.15	6
17.09	−101.22	10.17	11
17.11	−101.59	8.11	14
16.84	−101.32	8.21	34
16.98	−100.59	9.54	9
16.79	−101.39	9.15	4
16.98	−100.59	9.11	9
16.76	−101.29	9.32	40
17.06	−100.86	8.53	8
17.14	−100.82	10.21	4

the transition between locked (to the west) and creeping (to the east) interface segments.

Shallow LFEs were likely located at the plate interface in the Guerrero seismic gap. The distribution of the LFEs families shown in Fig. 7 suggests an interface dip angle of less than 10°, which is in reasonable agreement with previous investigations in Guerrero, suggesting a dip of 12 deg (Pacheco & Singh 2010). In general, the deep tremors and LFEs in Nankai, Mexico and Cascadia subduction zones are generally located on or around the plate interface. Toh *et al.* (2023) and Takemura *et al.* (2023) suggested that the difficulty in detecting shallow LFEs is due to the effects of low-velocity sediments beneath the OBSs (Takemura *et al.* 2020b). Although the depth error of shallow tremors where the distribution in the slab is relatively spread out is still large in our observations, the LFEs found in this study seem to occur on the plate interface, suggesting that similar physical processes and mechanisms of shallow tectonic tremors and deep tremors should be considered.

The specificity of earthquake activity in the Guerrero seismic gap makes us further consider the mechanisms of shallow slow earthquakes and the factors controlling their occurrence. Generally, fluids may play an auxiliary role by altering the conditions at the plate interface to enable transient slip events and tremor migration (Shelly *et al*. 2006; Cruz-Atienza *et al.* 2018; Warren-Smith *et al.* 2019). As mentioned above, a low residual gravity anomaly exists between the LFEs near the trench and beneath the coastline, around the -101° meridian (Fig. 1). Additionally, variations along the strike of the interface geometry and subducted seamounts around the Guerrero seismic gap may control LFEs and tremor activities. As shown in Fig. 1, the distributions of tremors and LFEs in the Guerrero seismic gap are correlated with the presence of seamounts and minimums in the residual gravity anomaly. This observation has also been made in other regions, where negative residual gravity anomalies are associated with small earthquakes and creep (Bassett & Watts 2015a, b).

The large positive and negative residual gravity anomalies have been interpreted as irregular subducting reliefs that increases pore pressure and fracturing and thus decreases coupling to generate shallow tremors (Plata-Martinez *et al.* 2021). Ide (2010) noted that deep tremors are influenced by the subduction of inhomogeneous structures, such as seamounts. Submarine geomorphic features on the active margin along the Mexican Pacific coast result from the subduction process (Černý *et al.* 2020). Large seamounts and basement reliefs cause permanent deformation when they collide with the overriding plates in subduction zones (Bangs *et al.* 2023). They may redistribute stress and reduce seismic slip. Small-scale fore-arc basins and seamounts have been found in the Guerrero seismic gap. The subducting topography drives marked spatial variations in tectonic loading, sediment consolidation and megathrust stress states (Sun *et al.* 2020). The distribution of slow earthquakes between OBS9 and OBS7 was clearly located over a large negative anomaly of gravity residuals anomaly that coincided with the locations of incoming and subducted seamounts (Figs 1 and 7). The same phenomenon was observed by Tomoda & Fujimoto (1981) in the Japanese subduction zone, where subducted seamounts were distributed in areas with negative gravity anomalies. When seamounts subduct, they leave behind a trail of soft sediments along the plate interface. Sediment patches help gradually release tectonic pressure during slow-slip earthquakes (Bangs *et al.* 2023).

The occurrence of tectonic tremors and shallow LFEs exhibited typical episodic features in the Guerrero seismic gap (Fig. 8). We observed three significant bursts of LFE occurrences in 2017 November, 2018 February and May (Fig. 8a). In general, tectonic tremors and LFEs occur episodically in temporal distributions, such as in Nankai, Cascadia, and Parkfield (Bostock *et al*. 2015; Shelly 2017; Kato & Nakagawa 2020).In contrast, small ordinary earthquakes are not characterized by such regularities in space and time, except for repeating earthquakes (Nadeau & Johnson 1998). Shallow tremors in the Guerrero seismic gap show episodic characteristics (Plata-Martinez *et al.* 2021), and the LFE are roughly distributed around the tremor, which can also be reflected in the tremor being composed of a series of LFEs (Shelly *et al.* 2007) (Fig. 1). This pattern bears a striking resemblance to the model of slow earthquakes in subduction zones summarized by Ito *et al.* (2007).

Around the Guerrero area, one evolution of the aseismic slip is in a northerly direction (Cruz-Atienza *et al.* 2021). At the same time, the aseismic slip region overlapped to some extent with the previous seismic rupture region. The area of overlap was the location where the LFEs numbered ID02, ID07 and ID12 were present (Fig. S7, Supporting Information). Fig. 8(b) shows the concentration of tremor occurrences near the trench in 2018 February. The temporal distribution of tremors suggests a southeast migration subparallel to the subduction zone axis (Figs 8b and c) along the along-strike transition zone bounding the seismic gap. In the diffusion model of slow earthquakes, the front location x and time t are typically related by the equation $x \propto \sqrt{t}$, more specially, this relationship can be expressed as $x = \sqrt{Dt}$, where D is the diffusion coefficient, within the range of diffusion coefficients by previous LFEs study (Kato & Nakagawa 2020) and tectonic tremors (Ide 2010; Ando *et al.* 2012). The migration of the tremors is shown in Fig. 8(c). Based on the diffusion equation of slow earthquakes, we calculated the coefficient D to be 1.0×10^4 m^2 s^{-1}. It is similar with Kato & Nakagawa (2020). The diffusion coefficient can quantify the rate at which this slip or tremor signal expands spatially. A high diffusion coefficient suggests that the slip or tremor is propagating rapidly over a large area, while a lower value indicates slower, more localized spreading.

5 CONCLUSION

This study analysed continuous seafloor seismic data in the Guerrero seismic gap from 2017–2019. We employed the envelope cross-correlation method to detect both long- and short-duration tremors and identified unreported tremors offshore the seismic gap. This facilitated the subsequent detection of LFEs also offshore, which were first discovered in this study. The LFE signals were curated by visual inspection within the tremor catalogue and further refined by waveform stacking in order to enhance the signal-to-noise ratio. Robust templates have been developed through iterative stacking and processing, enabling increased LFE detection via a template-matching strategy.

637 tectonic tremors and 205 LFEs have been successfully identified. The spatial and temporal clustering of these events aligned with the episodic nature of slow earthquakes. Notably, tectonic tremors were primarily detected near the trench, with significant activity observed at specific times, indicating southeastward migration parallel to the trench. Such tremor migration around the -101° meridian, which delineates the western end of the seismic gap, may reveal an along-strike plate interface transition zone preventing most of the large earthquakes to penetrate the gap from the adjacent segment. The LFEs were distributed close to and within the trench. The shallow LFEs did not always coincide with tremor activity, particularly near the trench.

Although initially active, tectonic tremors showed reduced activity over the subsequent two years, in contrast to other areas where activity remained stable. The spatial distribution of tectonic tremors as well as LFEs along the plate interface, indicates a shallow, trench-parallel transition zone from eastern creep to western lock, differing from the patterns observed in both the updip and downdip segments in other regions, such as the Nankai and Cascadia subduction zones. Notably, the occurrence of these seismic events correlates with geological features, such as seamounts and residual gravity anomalies, which appear to influence or even control slow earthquake mechanisms by altering the conditions on the plate interface.

ACKNOWLEDGMENTS

This research was supported by JSPS KAKENHI Grant Number JP21H05203 in Grant-in-Aid for Transformative Research Areas (A) 'Science of Slow-to-Fast Earthquakes' and JST in Japan Science and Technology Agency, the establishment of university

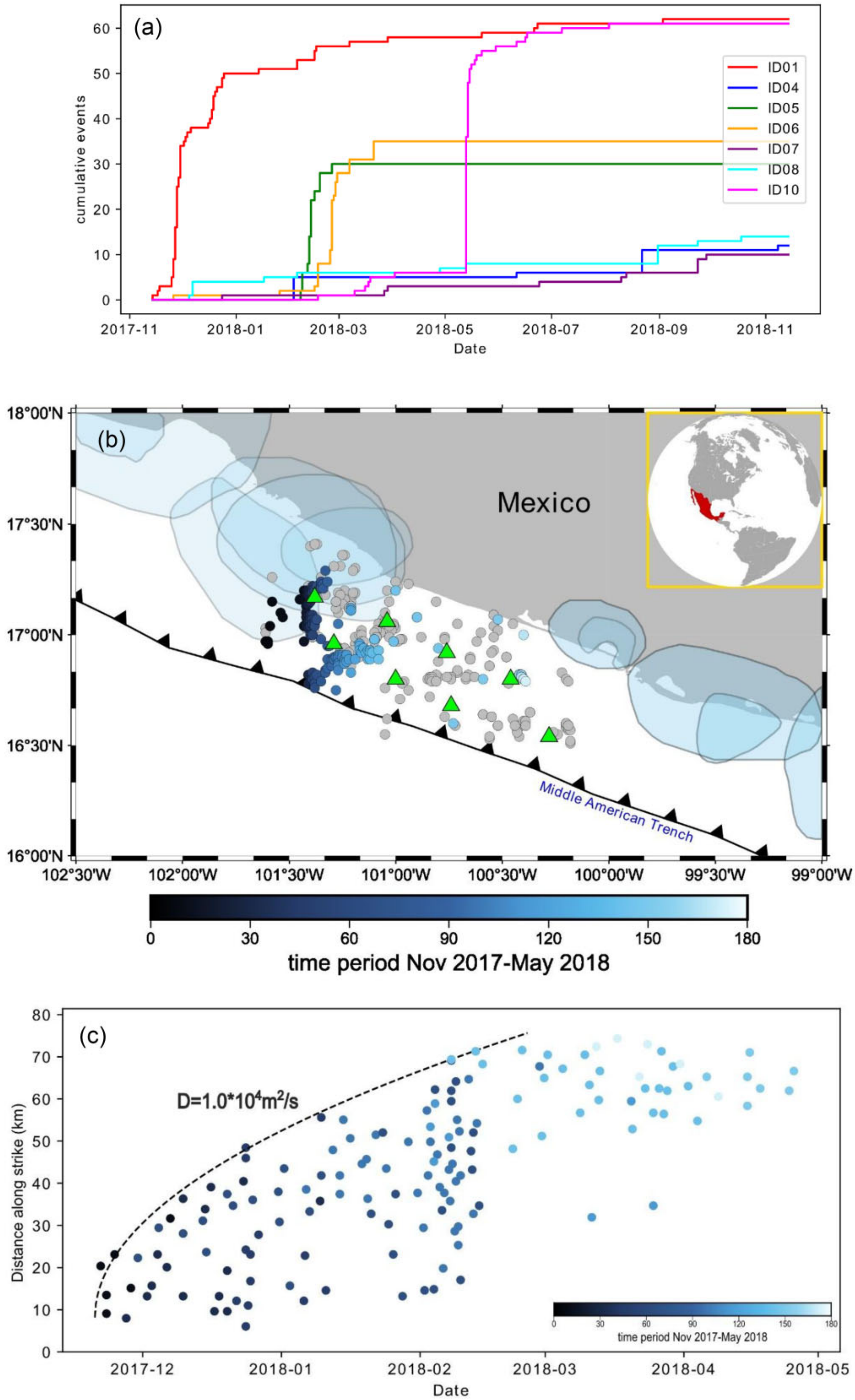

Figure 8. Panel (a) shows the cumulative number of the LFEs and daily LFEs count. The epicentre of different LFEs ID in Fig. S7 (Supporting Information). Panels (b) and (c) show the spatial and temporal migration of tremors in a selected period. The points that don't follow the colour bar gradient in panel (b) are tremors outside panel (c), while the points that change with the colour bar are tremors within panel (c).

fellowships towards the creation of science technology innovation, Grant Number JPMJFS2123. The work was also supported by Universidad Nacional Autónoma de México, Program for the Support of Research and Technological Innovation Projects (PAPIIT) grants IG100617, IG100921, IN111524 and R/V El Puma grants GGAP2017-1, GGAP2017-2, GGAP2018-1, GGAP2018-2 and GGAP2019. We thank editor John Hopper and Louise Alexander for their helpful suggestions and express thanks to Allen Husker and anonymous reviewer for their time and effort for improving the original manuscript. We thank Satoshi Ide and Naoto Mizuno for the modified envelope correlation code. We thank Zhigang Peng, Xiaofeng Meng and Dongdong Yao for sharing the MFT code and valuable discussion and David Shelly for constructive suggestions; and we also thank Chuan Li and Pousali Mukherjee for their helpful discussion.

SUPPORTING INFORMATION

Supplementary data are available at *GJIRAS* online.

Figure S1. One-dimensional velocity model beneath the subsurface structure we assumed.
Figure S2. Histogram of the tremor depth. The distribution of tremor depth is mainly around 10 km.
Figure S3. Workflow of the matched filter detecting.
Figure S4. One LFE within tremor shown on the horizontal and vertical components.
Figure S5. The initial location of those LFE candidate within tremors.
Figure S6. The number of tremor distributions, the colour of each block represents the number of tremors the block contains.
Figure S7. The epicentre of different LFEs ID in Fig. 8(a).

Please note: Oxford University Press is not responsible for the content or functionality of any supporting materials supplied by the authors. Any queries (other than missing material) should be directed to the corresponding author for the paper.

DATA AVAILABILITY

We use Python toolbox 'ObsPy' (Beyreuther *et al*. 2010) and Seismic Analysis Code (SAC; Goldstein & Snoke 2005) to process seismic data. We opened the LFE and tremor catalogue in the Supporting Information. The Code is available on request. Onshore data is available from SSN at: www.ssn.unam.mx. Ocean-bottom seismometer data from the SATREPS-UNAM project are subject to policies on restricted access. We used Generic Mapping Tools (Wessel *et al*. 2019), 'Matplotlib' (Hunter 2007) package and PyGMT (Uieda *et al.* 2021) to produce the figures.

REFERENCES

Akuhara, T., Yamashita, Y., Sugioka, H. & Shinohara, M., 2023. Locating tectonic tremors with uncertainty estimates: time-and amplitude-difference optimization, wave propagation-based quality control and bayesian inversion, *Geophys. J. Int.,* **235**(3), 2727–2742.

Ando, M., Tu, Y., Kumagai, H., Yamanaka, Y. & Lin, C.H., 2012. Very low frequency earthquakes along the Ryukyu subduction zone, *Geophys. Res. Lett.,* **39**(4), 2011GL050559. https://doi.org/10.1029/2011GL050559.

Arai, R. *et al.* 2016. Structure of the tsunamigenic plate boundary and low-frequency earthquakes in the southern Ryukyu Trench, *Nat. Commun.,* **7**(1), 12255. https://doi.org/10.1038/ncomms12255.

Asano, Y., Obara, K. & Ito, Y., 2008. Spatiotemporal distribution of very-low frequency earthquakes in Tokachi-oki near the junction of the Kuril and Japan trenches revealed by using array signal processing, *Earth Planets Space,* **60,** 871–875.

Baba, S., Obara, K., Takemura, S., Takeo, A. & Abers, G.A., 2021. Shallow slow earthquake episodes near the trench axis off Costa Rica, *J. Geophys. Res. Solid Earth,* **126**(9), e2021JB021706. https://doi.org/10.1029/2021JB021706.

Baba, S., Takemura, S., Obara, K. & Noda, A., 2020. Slow earthquakes illuminating interplate coupling heterogeneities in subduction zones, *Geophys. Res. Lett.,* **47**(14), e2020GL088089. https://doi.org/10.1029/2020GL088089.

Bangs, N.L. *et al.* 2023. Slow slip along the Hikurangi margin linked to fluid-rich sediments trailing subducting seamounts, *Nat. Geosci.,* **16**(6), 505–512.

Bartlow, N.M., Miyazaki, S.I., Bradley, A.M. & Segall, P., 2011. Space-time correlation of slip and tremor during the 2009 Cascadia slow slip event, *Geophys. Res. Lett.,* **38**(18), https://doi.org/10.1029/2011GL048714.

Bassett, D. & Watts, A.B., 2015a. Gravity anomalies, crustal structure, and seismicity at subduction zones: 1. Seafloor roughness and subducting relief, *Geochem. Geophys. Geosyst.,* **16**(5), 1508–1540.

Bassett, D. & Watts, A.B., 2015b. Gravity anomalies, crustal structure, and seismicity at subduction zones: 2. Interrelationships between fore-arc structure and seismogenic behaviour, *Geochem. Geophys. Geosyst.,* **16**(5), 1541–1576.

Beaucé, E., Frank, W.B. & Romanenko, A., 2018. Fast matched filter (FMF): an efficient seismic matched-filter search for both CPU and GPU architectures, *Seismol. Res. Lett.,* **89**(1), 165–172.

Beck, J.L. & Hall, J.F., 1986. Factors contributing to the catastrophe in Mexico City during the earthquake of 1985 September 19, *Geophys. Res. Lett.,* **13**(6), 593–596.

Bell, S., Ruan, Y. & Forsyth, D.W., 2016. Ridge asymmetry and deep aqueous alteration at the trench observed from Rayleigh wave tomography of the Juan de Fuca plate, *J. Geophys. Res. Solid Earth,* **121**(10), 7298–7321.

Beroza, G.C. & Ide, S., 2011. Slow earthquakes and nonvolcanic tremor, *Annu. Rev. Earth Planet. Sci.,* **39,** 271–296.

Beyreuther, M., Barsch, R., Krischer, L., Megies, T., Behr, Y. & Wassermann, J., 2010. ObsPy: A Python toolbox for seismology. *Seismol. Res. Lett.,* **81**(3), 530–533.

Bostock, M.G., Thomas, A.M., Savard, G., Chuang, L. & Rubin, A.M., 2015. Magnitudes and moment-duration scaling of low-frequency earthquakes beneath southern Vancouver Island, *J. Geophys. Res.: Solid Earth* **120**(9), 6329–6350.

Brown, J.R. *et al.* 2009. Deep low-frequency earthquakes in tremor localize to the plate interface in multiple subduction zones, *Geophys. Res. Lett.,* **36**(19), https://doi.org/10.1029/2009GL040027.

Černý, J., Ramírez-Herrera, M.T., Garcia, E.S. & Ito, Y., 2020. Seafloor morphology along the active margin in Guerrero, Mexico: probable earthquake implications, *J. South Amer. Earth Sci.,* **102,** 102671. https://doi.org/10.1016/j.jsames.2020.102671.

Chamberlain, C.J., Boese, C.M. & Townend, J., 2017. Cross-correlation-based detection and characterization of microseismicity adjacent to the locked, late-interseismic Alpine Fault, South Westland, New Zealand, *Earth planet. Sci. Lett.,* **457,** 63–72.

Chamberlain, C.J., Shelly, D.R., Townend, J. & Stern, T.A., 2014. Low-frequency earthquakes reveal punctuated slow slip on the deep extent of the Alpine Fault, New Zealand, *Geochem. Geophys. Geosyst.,* **15**(7), 2984–2999.

Chow, B., Kaneko, Y., Tape, C., Modrak, R., Mortimer, N., Bannister, S. & Townend, J., 2022. Strong upper-plate heterogeneity at the Hikurangi subduction margin (North Island, New Zealand) imaged by adjoint tomography, *J. Geophys. Res. Solid Earth,* **127**(1), e2021JB022865. https://doi.org/10.1029/2021JB022865.

Cruz-Atienza, V.M. *et al.* 2018. A seismogeodetic amphibious network in the Guerrero seismic gap, Mexico, *Seismol. Res. Lett.,* **89**(4), 1435–1449.

Cruz-Atienza, V.M. *et al.* 2021. Short-term interaction between silent and devastating earthquakes in Mexico, *Nat. Commun.,* **12**(1), 2171. https://doi.org/10.1038/s41467-021-22326-6.

Cruz-Atienza, V.M., Husker, A., Legrand, D., Caballero, E. & Kostoglodov, V., 2015. Nonvolcanic tremor locations and mechanisms in Guerrero, Mexico, from energy-based and particle motion polarization analysis, *J. Geophys. Res. Solid Earth,* **120**(1), 275–289.

Cruz-Atienza, V.M., Villafuerte, C. & Bhat, H.S., 2018. Rapid tremor migration and pore-pressure waves in subduction zones, *Nat. Commun.,* **9**(1), 2900. https://doi.org/10.1038/s41467-018-05150-3.

Dixon, T.H., Jiang, Y., Malservisi, R., McCaffrey, R., Voss, N., Protti, M. & Gonzalez, V. 2014. Earthquake and tsunami forecasts: relation of slow slip events to subsequent earthquake rupture, *Proc. Natl. Acad. Sci. USA,* **111**(48), 17 039–17 044.

Efron, B. 1979. Bootstrap methods: another look at the jackknife, *Ann. Stat.,* **7**(1), 1–26.

Espindola-Carmona, A., Peter, D. & Ortiz-Aleman, C., 2021. Crustal and upper-mantle structure below Central and southern Mexico, *J. Geophys. Res. Solid Earth,* **126**(6), e2020JB020906. https://doi.org/10.1029/2020jb020906.

Frank, W.B., Shapiro, N.M., Husker, A.L., Kostoglodov, V., Romanenko, A. & Campillo, M., 2014. Using systematically characterized low-frequency earthquakes as a fault probe in Guerrero, Mexico, *J. Geophys. Res. Solid Earth,* **119**(10), 7686–7700.

Frank, W.B., Shapiro, N.M., Kostoglodov, V., Husker, A.L., Campillo, M., Payero, J.S. & Prieto, G.A., 2013. Low-frequency earthquakes in the Mexican Sweet Spot, *Geophys. Res. Lett.,* **40**(11), 2661–2666.

Gibbons, S.J. & Ringdal, F., 2006. The detection of low magnitude seismic events using array-based waveform correlation, *Geophys. J. Int.,* **165**(1), 149–166.

Goldstein, P.A.U.L. & Snoke, A., 2005. SAC availability for the IRIS community, *Incorporated Research Institutions for Seismology Newsletter,* **7,** UCRL-JRNL-211140.

Gombert, B. & Hawthorne, J.C., 2023. Rapid tremor migration during few minute-long slow earthquakes in Cascadia, *J. Geophys. Res.: Solid Earth,* **128**(2), 2022JB025034. https://doi.org/10.1029/2022JB025034.

Hayes, G.P., Moore, G.L., Portner, D.E., Hearne, M., Flamme, H., Furtney, M. & Smoczyk, G.M., 2018. Slab2, a comprehensive subduction zone geometry model, *Science,* **362**(6410), 58–61.

Hendriyana, A. & Tsuji, T., 2021. Influence of structure and pore pressure of plate interface on tectonic tremor in the Nankai subduction zone, Japan, *Earth planet. Sci. Lett.,* **558,** 116 742.

Hirata, N. & Matsu'ura, M., 1987. Maximum-likelihood estimation of hypocenter with origin time eliminated using nonlinear inversion technique, *Phys. Earth planet. Inter.,* **47,** 50–61.

Hirose, H. & Obara, K., 2005. Repeating short-and long-term slow slip events with deep tremor activity around the Bungo channel region, southwest Japan. *Earth, planets and space* **57,** 961–972. https://doi.org/10.1186/BF03351875.

Hjörleifsdóttir, V., Singh, S. & Husker, A., 2016. Differences in epicentral location of Mexican earthquakes between local and global catalogs: an update, *Geofis. Int.,* **55**(1), 79–93. https://doi.org/10.22201/igeof.00167169p.2016.55.1.1713.

Hunter, J.D., 2007. Matplotlib: a 2D graphics environment, *Comput. Sci. Eng.,* **9**(03), 90–95.

Husker, A., Frank, W.B., Gonzalez, G., Avila, L., Kostoglodov, V. & Kazachkina, E. 2019. Characteristic tectonic tremor activity observed over multiple slow slip cycles in the Mexican subduction zone, *J. Geophys. Res. Solid Earth,* **124**(1), 599–608.

Husker, A.L., Kostoglodov, V., Cruz-Atienza, V.M., Legrand, D., Shapiro, N.M., Payero, J.S., Campillo, M. & Huesca-Pérez, E., 2012. Temporal variations of non-volcanic tremor (NVT) locations in the Mexican subduction zone: finding the NVT sweet spot, *Geochem. Geophys. Geosyst.,* **13**(3), 2011GC003916. https://doi.org/10.1029/2011GC003916.

Ide, S., 2010. Striations, duration, migration and tidal response in deep tremor, *Nature,* **466**(7304), 356–359.

Ide, S., 2021. Empirical low-frequency earthquakes synthesized from tectonic tremor records, *J. Geophys. Res. Solid Earth,* **126**(12), e2021JB022498. https://doi.org/10.1029/2021JB022498.

Ide, S., Shelly, D.R. & Beroza, G.C., 2007. Mechanism of deep low frequency earthquakes: Further evidence that deep non-volcanic tremor is generated by shear slip on the plate interface, *Geophys. Res. Lett.,* **34**(3), 2006GL028890. https://doi.org/10.1029/2006GL028890.

Iglesias, A., Singh, S., Pacheco, J., Alca´ntara, L., Ortiz, M. & Ordaz, M., 2003. Near-trench Mexican earthquakes have anomalously low peak accelerations.*Bull. seism Soc. Am.,* **93**(2), 953–959. https://doi.org/10.1785/0120020168.

Ito, Y., *et al.* 2013. Episodic slow slip events in the Japan subduction zone before the 2011 Tohoku-Oki earthquake, *Tectonophysics,* **600,** 14–26.

Ito, Y., Hino, R., Suzuki, S. & Kaneda, Y., 2015. Episodic tremor and slip near the Japan Trench prior to the 2011 Tohoku-Oki earthquake, *Geophys. Res. Lett.,* **42**(6), 1725–1731.

Ito, Y., Obara, K., Shiomi, K., Sekine, S. & Hirose, H., 2007. Slow earthquakes coincident with episodic tremors and slow slip events, *Science,* **315**(5811), 503–506.

Itoh, Y., Aoki, Y. & Fukuda, J. 2022. Imaging evolution of Cascadia slow-slip event using high-rate GPS, *Sci. Rep.,* **12**(1), 7179. https://doi.org/10.1038/s41598-022-10957-8.

Kanamori, H., Jennings, P.C., Singh, S.K. & Astiz, L., 1993. Estimation of strong ground motions in Mexico City expected for large earthquakes in the Guerrero seismic gap, *Bull. seism. Soc. Am.,* **83**(3), 811–829.

Kato, A. & Nakagawa, S., 2020. Detection of deep low-frequency earthquakes in the Nankai subduction zone over 11 years using a matched filter technique, *Earth Planets Space,* **72,** 128. https://doi.org/10.1186/s40623-020-01257-4.

Kato, A., Obara, K., Igarashi, T., Tsuruoka, H., Nakagawa, S. & Hirata, N., 2012. Propagation of slow slip leading up to the 2011 M w 9.0 Tohoku-Oki earthquake, *Science,* **335**(6069), 705–708.

Kostoglodov, V., Husker, A., Shapiro, N.M., Payero, J.S., Campillo, M., Cotte, N. & Clayton, R., 2010. The 2006 slow slip event and nonvolcanic tremor in the Mexican subduction zone, *Geophys. Res. Lett.,* **37**(24), 2010GL045424. https://doi.org/10.1029/2010GL045424,

Kostoglodov, V., Singh, S.K., Santiago, J.A., Franco, S.I., Larson, K.M., Lowry, A.R. & Bilham, R., 2003. A large silent earthquake in the Guerrero seismic gap, Mexico, *Geophys. Res. Lett.,* **30**(15). 2003GL017219. https://doi.org/10.1029/2003GL017219.

Maceira, M., Rowe, C.A., Beroza, G. & Anderson, D., 2010. Identification of low-frequency earthquakes in non-volcanic tremor using the subspace detector method, *Geophys. Res. Lett.,* **37**(6), 2009GL041876. https://doi.org/10.1029/2009GL041876.

Matsuzawa, T., Asano, Y. & Obara, K., 2015. Very low frequency earthquakes off the Pacific coast of Tohoku, Japan, *Geophys. Res. Lett.,* **42**(11), 4318–4325.

Meng, X., Peng, Z. & Hardebeck, J.L., 2013. Seismicity around Parkfield correlates with static shear stress changes following the 2003 Mw 6. 5 San Simeon earthquake, *J. Geophys. Res. Solid Earth,* **118**(7), 3576–3591.

Mizuno, N. & Ide, S., 2019. Development of a modified envelope correlation method based on maximum-likelihood method and application to detecting and locating deep tectonic tremors in western Japan, *Earth Planets Space,* **71,** 40. https://doi.org/10.1186/s40623-019-1022-x.

Nadeau, R.M. & Johnson, L.R., 1998. Seismological studies at Parkfield VI: Moment release rates and estimates of source parameters for small repeating earthquakes, *Bull. Seismol. Soc. Am.,* **88**(3), 790–814.

Nakamura, M., 2017. Distribution of low-frequency earthquakes accompanying the very low frequency earthquakes along the Ryukyu Trench. *Earth, Planets and Space,* **69,** 49. https://doi.org/10.1186/s40623-017-0632-4

Nishikawa, T., Matsuzawa, T., Ohta, K., Uchida, N., Nishimura, T. & Ide, S. 2019. The slow earthquake spectrum in the Japan Trench illuminated by the S-net seafloor observatories, *Science,* **365**(August), 808–813.

Obana, K., Kodaira, S., Kaneda, Y., Mochizuki, K., Shinohara, M. & Suyehiro, K., 2003. Microseismicity at the seaward updip limit of the western Nankai Trough seismogenic zone, *J. Geophys. Res. Solid Earth,* **108**(B10), 2002JB002370. https://doi.org/10.1029/2002JB002370.

Obara, K. & Ito, Y., 2005. Very low frequency earthquake excited by the 2004 off the Kii peninsula earthquake: a dynamic deformation process in the large accretionary prism, *Earth Planets Space,* **57**(4), 321–326.

Obara, K. & Kato, A., 2016. Connecting slow earthquakes to huge earthquakes, *Science,* **353**(6296), 253–257.

Obara, K., 2002. Nonvolcanic deep tremor associated with subduction in southwest Japan, *Science,* **296**(5573), 1679–1681.

Obara, K., 2020. Characteristic activities of slow earthquakes in Japan, *Proc. Jpn. Acad. Ser. B,* **96**(7), 297–315.

Ohta, K. & Ide, S., 2011. Precise hypocentre distribution of deep low-frequency earthquakes and its relationship to the local geometry of the subducting plate in the Nankai subduction zone, Japan, *J. Geophys. Res. Solid Earth,* **116**(B1), https://doi.org/10.1029/2010JB007857.

Okal, E.A., 2008. The generation of T waves by earthquakes, *Adv. Geophys.,* **49,** 1–65.

Pacheco, J.F. & Singh, S.K., 2010. Seismicity and state of stress in Guerrero segment of the Mexican subduction zone, *J. Geophys. Res. Solid Earth,* **115**(B1), 2009JB006453. https://doi.org/10.1029/2009jb006453.

Payero, J.S., Kostoglodov, V., Shapiro, N., Mikumo, T., Iglesias, A., Pérez-Campos, X. & Clayton, R.W., 2008. Nonvolcanic tremor observed in the Mexican subduction zone, *Geophys. Res. Lett.,* **35**(7), 2007GL032877. https://doi.org/10.1029/2007GL032877.

Peng, Z. & Zhao, P., 2009. Migration of early aftershocks following the 2004 Parkfield earthquake, *Nat. Geosci.,* **2**(12), 877–881.

Plata-Martínez, R. *et al.* 2021. Shallow slow earthquakes to decipher future catastrophic earthquakes in the Guerrero seismic gap, *Nat. Commun.,* **12**(1), 3976. https://doi.org/10.1038/s41467-021-24210-9.

Poiata, N., Vilotte, J.P., Bernard, P., Satriano, C. & Obara, K., 2018. Imaging different components of a tectonic tremor sequence in southwestern Japan using an automatic statistical detection and location method, *Geophys. J. Int.,* **213**(3), 2193–2213.

Radiguet, M. *et al.* 2016. Triggering of the 2014 Mw 7.3 Papanoa earthquake by a slow slip event in Guerrero, Mexico, *Nat. Geosci.,* **9**(11), 829–833.

Radiguet, M., Cotton, F., Vergnolle, M., Campillo, M., Walpersdorf, A., Cotte, N. & Kostoglodov, V., 2012. Slow slip events and strain accumulation in the Guerrero gap, Mexico, *J. Geophys. Res. Solid Earth,* **117**(B4), 2011JB008801. https://doi.org/10.1029/2011JB008801.

Rogers, G. & Dragert, H., 2003. Episodic tremor and slip on the Cascadia subduction zone: The chatter of silent slip, *Science,* **300**(5627), 1942–1943.

Servicio Sismológico Nacional (SSN), Servicio Sismológico Nacional, Instituto de Geofísica, Universidad Nacional Autónoma de México 2018.

Shelly, D.R., 2017. A 15 year catalogue of more than 1 million low-frequency earthquakes: tracking tremor and slip along the deep San Andreas Fault, *J. Geophys. Res. Solid Earth,* **122**(5), 3739–3753.

Shelly, D.R., Beroza, G.C. & Ide, S., 2007. Non-volcanic tremor and low-frequency earthquake swarms, *Nature,* **446**(7133), 305–307.

Shelly, D.R., Beroza, G.C., Ide, S. & Nakamula, S., 2006. Low-frequency earthquakes in Shikoku, Japan and their relationship to episodic tremor and slip, *Nature,* **442,** 188–191.

Shelly, D.R., Ellsworth, W.L., Ryberg, T., Haberland, C., Fuis, G.S., Murphy, J., Nadeau, R.M. & Bürgmann, R., 2009. Precise location of San Andreas fault tremors near Cholame, California using seismometer clusters: Slip on the deep extension of the fault?, *Geophys. Res. Lett.,* **36**(1), 2008GL036367. https://doi.org/10.1029/2008GL036367.

Singh, S.K., Astiz, L. & Havskov, J., 1981. Seismic gaps and recurrence periods of large earthquakes along the Mexican subduction zone: a reexamination, *Bull. seism. Soc. Am.,* **71**(3), 827–843.

Singh, S.K., Plata-Martínez, R., Pérez-Campos, X., Espíndola, V.H., Arroyo, D. & Iglesias, A., 2019. Evidence of directivity during the earthquakes of 8 and 10 May 2014 (Mw 6.5, 6.1) in the Guerrero, Mexico seismic gap and some implications, *J. Seismol.,* **23,** 683–697.

Spica, Z., Perton, M., Calò, M., Legrand, D., Córdoba-Montiel, F. & Iglesias, A., 2016. 3-D shear wave velocity model of Mexico and South US: bridging seismic networks with ambient noise cross-correlations (C1) and correlation of coda of correlations (C 3), *Geophys. J. Int.,* **206**(3), 1795–1813.

Sun, T., Saffer, D. & Ellis, S., 2020. Mechanical and hydrological effects of seamount subduction on megathrust stress and slip, *Nat. Geosci.,* **13**(3), 249–255.

Supino, M., Poiata, N., Festa, G., Vilotte, J.P., Satriano, C. & Obara, K. 2020. Self-similarity of low-frequency earthquakes, *Sci. Rep.,* **10**(1), 6523.

Svanberg, K., 2002. A class of globally convergent optimization methods based on conservative convex separable approximations, *SIAM J. Optim.,* **12**(2), 555–573.

Takemura, S., Emoto, K. & Yabe, S., 2024a. Revisiting seismic energy of shallow tremors: amplifications due to site and propagation path effects near the Nankai Trough, *J. Geophys. Res. Solid Earth,* **129**(6), e2024JB029168. https://doi.org/10.1029/2024JB029168.

Takemura, S., Hamada, Y., Okuda, H., Okada, Y., Okubo, K., Akuhara, T., Noda, A. & Tonegawa, T., 2023. A review of shallow slow earthquakes along the Nankai Trough, *Earth Planets Space,* **75**(1), 164. https://doi.org/10.1186/s40623-023-01920-6.

Takemura, S., Kubota, T. & Sandanbata, O., 2024b. Successive tsunamigenic events near Sofu seamount inferred from high-frequency teleseismic P and regional T waves, *J. Geophys. Res. Solid Earth,* **129**(10), e2024JB029746. https://doi.org/10.1029/2024JB029746.

Takemura, S., Okuwaki, R., Kubota, T., Shiomi, K., Kimura, T. & Noda, A., 2020a. Centroid moment tensor inversions of offshore earthquakes using a three-dimensional velocity structure model: slip distributions on the plate boundary along the Nankai Trough, *Geophys. J. Int.,* **222**(2), 1109–1125.

Takemura, S., Yabe, S. & Emoto, K., 2020b. Modelling high-frequency seismograms at ocean bottom seismometers: effects of heterogeneous structures on source parameter estimation for small offshore earthquakes and shallow low-frequency tremors, *Geophys. J. Int.,* **223**(3), 1708–1723.

Tang, C.C., Peng, Z., Chao, K., Chen, C.H. & Lin, C.H., 2010. Detecting low-frequency earthquakes within non-volcanic tremor in southern Taiwan triggered by the 2005 Mw 8.6 Nias earthquake, *Geophys. Res. Lett.,* **37**(16), 2010GL043918. https://doi.org/10.1029/2010GL043918.

Thurber, C.H., Zeng, X., Thomas, A.M. & Audet, P., 2014. Phase-weighted stacking applied to low-frequency earthquakes, *Bull. seism. Soc. Am.,* **104**(5), 2567–2572.

Todd, E.K. *et al.* 2018. Earthquakes and tremor linked to seamount subduction during shallow slow slip at the Hikurangi margin, New Zealand, *J. Geophys. Res. Solid Earth,* **123**(8), 6769–6783.

Toh, A., Capdeville, Y., Chi, W.C. & Ide, S., 2023. Strongly scattering medium along slow earthquake fault zones based on new observations of short-duration tremors, *Geophys. Res. Lett.,* **50**(8), e2022GL101851. https://doi.org/10.1029/2022GL101851.

Tomoda, Y. & Fujimoto, H., 1981. Gravity anomalies in the western Pacific and geophysical interpretation of their origin, *J. Phys. Earth,* **29**(5), 387–419.

Uchida, N., Iinuma, T., Nadeau, R.M., Bürgmann, R. & Hino, R., 2016. Periodic slow slip triggers megathrust zone earthquakes in northeastern Japan, *Science,* **351**(6272), 488–492.

Uieda, L. *et al.* 2021. PyGMT: a Python interface for the generic mapping tools, https://doi.org/10.5281/zenodo.4978645.

UNAM Seismology Group, 1986. The September 1985 Michoacán earthquakes: aftershock distribution and history of rupture, *Geophys. Res. Lett.,* **13**(6), 573–576.

UNAM Seismology Group. 2015. Papanoa, Mexico earthquake of 18 April 2014 (Mw 7.3), *Geofis. Int.,* **54**(4), 363–386.

Urabe, T., 1992. win-A workstation program for processing waveform data from microearthquake networks. *Abstr. Seismol. Soc. Jpn.,* Vol. **2,** p. 331).

Villafuerte, C. & Cruz-Atienza, V.M., 2017. Insights into the causal relationship between slow slip and tectonic tremor in Guerrero, Mexico, *J. Geophys. Res. Solid Earth,* **122**(8), 6642–6656.

Warren-Smith, E. *et al.* 2019. Episodic stress and fluid pressure cycling in subducting oceanic crust during slow slip, *Nat. Geosci.,* **12**(6), 475–481.

Wech, A.G. & Bartlow, N.M., 2014. Slip rate and tremor genesis in Cascadia, *Geophys. Res. Lett.,* **41**(2), 392–398.

Wech, A.G., 2021. Cataloging tectonic tremor energy radiation in the Cascadia subduction zone, *J. Geophys. Res. Solid Earth,* **126**(10), e2021JB022523. https://doi.org/10.1029/2021JB022523.

Wessel, P., Luis, J.F., Uieda, L.A., Scharroo, R., Wobbe, F., Smith, W.H. & Tian, D., 2019. The generic mapping tools version 6 *Geochem. Geophys. Geosyst.,* **20**(11), 5556–5564.

Yabe, S., Baba, S., Tonegawa, T., Nakano, M. & Takemura, S., 2021. Seismic energy radiation and along-strike heterogeneities of shallow tectonic tremors at the Nankai Trough and Japan Trench, *Tectonophysics,* **800,** 228714. https://doi.org/10.1016/j.tecto.2020.228714.

Yabe, S., Tonegawa, T. & Nakano, M., 2019. Scaled energy estimation for shallow slow earthquakes, *J. Geophys. Res. Solid Earth,* **124**(2), 1507–1519.

Yao, D., Walter, J.I., Meng, X., Hobbs, T.E., Peng, Z., Newman, A.V., Schwartz, S.Y. & Protti, M., 2017. Detailed spatiotemporal evolution of microseismicity and repeating earthquakes following the 2012 Mw 7.6 Nicoya earthquake, *J. Geophys. Res. Solid Earth,* **122**(1), 524–542.

Yoshioka, S., Mikumo, T., Kostoglodov, V., Larson, K.M., Lowry, A.R. & Singh, S.K., 2004. Interplate coupling and a recent aseismic slow slip event in the Guerrero seismic gap of the Mexican subduction zone, as deduced from GPS data inversion using a Bayesian information criterion, *Phys. Earth Planet. Inter.,* **146**(3-4), 513–530.